PARAMETRIC INVESTIGATION OF A GRAPHITE FOAM EVAPORATOR IN A THERMOSYPHON WITH FLUORINERT™ AND A SILICON CMOS CHIP

James W. Klett, Michael Trammell
Metals and Ceramics Division, Oak Ridge National Laboratory, Oak Ridge, TN, 37831

Abstract

High thermal conductivity graphitic foam was utilized as the evaporator in a modified thermosyphon. The foam was soldered directly to the back of a silicon CMOS die and mounted in a standard PGA. Fluorinert™ FC-87 and FC-72 were evaluated as the working fluids of choice and a variety of variables on the foams were explored. It was found that the density of the foam evaporators affected the thermal performance of the system. However, the fluid level and fluid type had very little effect on the overall performance in the system, making fabrication of a commercial device less challenging.

The most significant effect on performance was the modifications to the foam structure. Slotted patterns were found to enhance the rate of return of fluid to the foam closest to the die, thus improving performance. With a slotted foam evaporator, a heat flux of $150 W/cm^2$ resulted in wall superheats of only 11°C.

The experimental setup used in this research gives accurate measurements of the actual active layer in the chip and temperatures less than 71°C have been achieved at heat fluxes of $150 W/cm^2$. This performance is significantly better than any prior literature data. In fact, the graphite foam thermosyphons were shown to outperform spray cooling. In addition, it was found that critical heat flux was not reached in these experiments with graphite foam evaporators at heat fluxes as high as $150 W/cm^2$.

1. Introduction

Current CMOS (complementary metal-oxide semiconductors) type microprocessors experience power densities up to $50 W/cm^2$ and are cooled effectively with aluminum and copper heat sinks. However, as technology improves, high performance computer chips will likely experience power densities over $200 W/cm^2$. Currently, the only commercially viable cooling technology capable of handling this high demand with chips is spray cooling [1, 2]. For comparison, the leading edge of the space shuttle orbiter experiences $40 W/cm^2$ upon re-entry. However, while spray cooling has demonstrated high cooling capacities, costs, reliability and repair are serious concerns. Today, spray cooling is limited to devices where performance is critical. Over the last decade or so, researchers have been exploring passive and lower cost alternative methods for cooling computer chips and other high power density devices such as power electronics [3-10].

[1]The "flip-chip" design currently used in today's microprocessors has inherent problems. Here, the silicon die is inverted with the back of the printed chip oriented

towards the top of the package. In this case, the integrated heat spreader (IHS) can be joined (typically with epoxy) directly to the silicon chip and cooled with a finned air cooled heat sink. Unfortunately, as the power increases above 100W, this can result in temperatures above design limits on the printed active layer in the chip, reducing reliability and shortening life.

Current research and has focus on the thermosyphon design where the heat sink bonded to the chip is immersed in an evaporative cooling fluid (e.g. fluorocarbon, FC-87, FC-72). [4-10]. The latent heat of vaporization of the cooling fluid removes significantly more heat than the sensible heat change of the fluid while transferring the heat efficiently to fins of a condenser. The performance of the evaporative coolers is currently limited by the surface area and thermal conductivity of the spreader mounted to the back of the chip.

The National Security Agency (NSA) has conducted research on thermosyphons using state of the art polycrystalline diamond wafers with thermal conductivities up to 1600 W/m·K (about 4 times that of copper) as the heat spreader. As a result of the limited surface area of the diamond spreader, the maximum power density achieved without over heating the system was 28 W/cm^2 [11]. On the other hand, Ramaswamy [6], et al, evaluated the use of a microchannel copper evaporator to improve the surface area, however the thermal conductivity of the evaporator was sacrificed (a porous material is never as conductive as the solid). Heat fluxes of up to 100 W/cm^2 were demonstrated at a wall superheat, ΔT_{SH} (the temperature difference between the back of the evaporator, T_{wall}, and the evaporative fluid, T_{sat}), greater than 65°C. Nakayama, et al, demonstrated heat fluxes up to 159 W/cm^2 at wall superheats of 65°C using a similar microchannel evaporator [10]. However, the two techniques with the high power densities do not consider the temperature rise across the stack-up of the silicon die and any adhesive interfaces ($T_{active} - T_{wall}$).

Collaborative research by National Security Agency, the Laboratory for Physical Sciences (LPS), and the Oak Ridge National Laboratory (ORNL), has resulted in the demonstration of novel techniques for cooling electronic integrated chips with very high power densities involving alternative evaporators. High thermal conductivity graphitic foam, developed and patented by ORNL under the direction of the U.S. Department of Energy (DOE) Office of Transportation Technologies, when used as a heat spreader improves both the surface area and thermal conductivity versus industry standards. The lightweight foam has a high bulk thermal conductivity (up to 180 W/m·K), and an open porous structure (Figure 1) with more than 2 orders of magnitude greater surface area than the state-of-the-art diamond wafers currently utilized as heat spreaders. The cell walls are made of oriented graphitic planes and exhibit thermal conductivities in excess of 1640 W/m·K [12-17]. Hence, the foam acts as a microporous heat spreader with significantly more surface area and more than 4 times the solid conductivity compared to the evaporator in Ramaswamy. Even more impressive is that this is more than ten times that of the conductivity of the silicon itself.
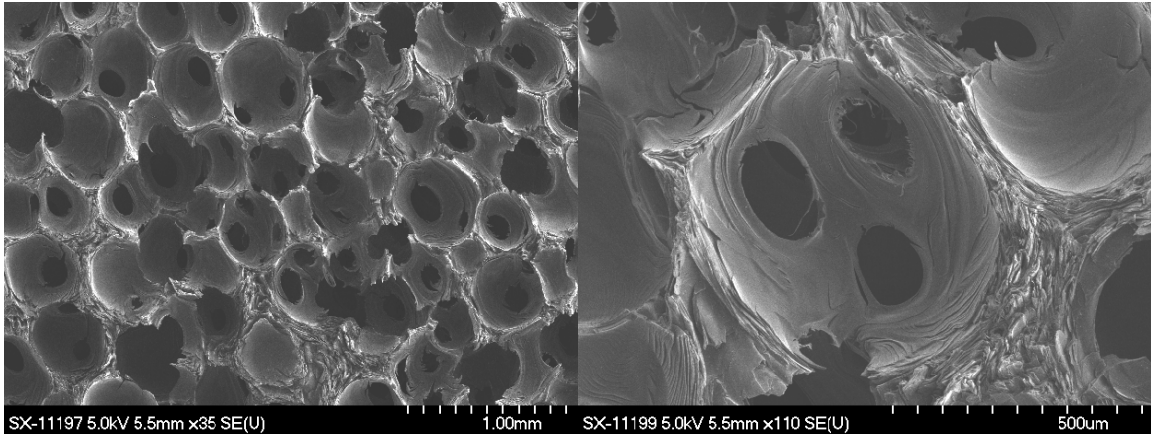
Figure 1. Scanning electron microscopy images of the graphite foam.

2. Experimental setup and conduct

2.1. Experimental setup

The system developed to investigate microelectronic CMOS chip cooling, shown in Figure 2, consists of the following components: (a) a silicon die with a resistor as the printed active layer, (b) a block of graphite foam measuring 2.5x2.5x1cm mounted to the chip by soldering (c) a pin grid array (PGA) mounted and wire bonded to the chip by Laboratory for Physical Sciences (LPS), (d) an aluminum holder attached to the chip assembly using RTV sealant, (e) a zero insertion force (ZIF) socket attached to a circuit board, (f) a circuit board and wiring, (g) a glass walled chamber with aluminum flanges, (h) a fluid bubbler for de-airing the Fluorinert, (i) a water cooled condenser, (j) a 1000W power supply, (k) type-K thermocouples, (l) 4 multimeters for measuring resistance of resistors printed on the active layer, (m) Swagelok valve and fittings.
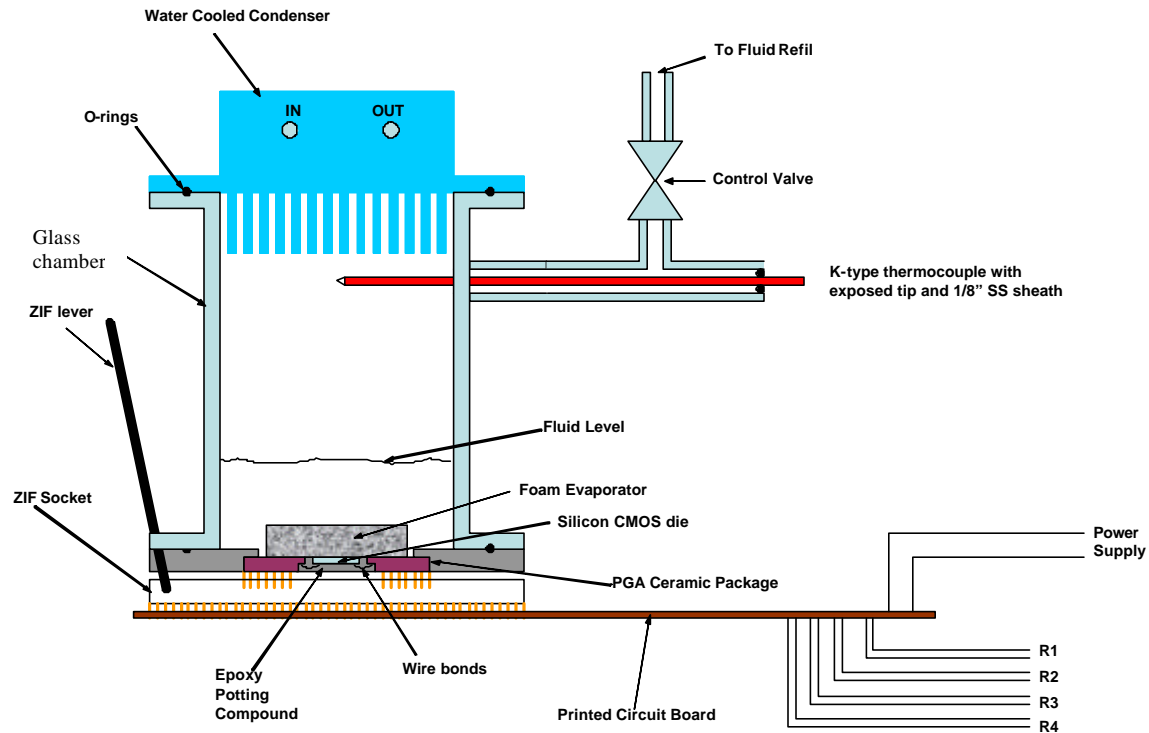
Figure 2.   Schematic of setup

The silicon die, Figure 3a, has two independent resistors used to heat the chip with a very linear heating profile. In addition, it has 4 independent resistors printed on the active layers which, when monitored during operation, can be directly correlated to temperature of the printed active layer. Therefore, the temperature rise across the chip can be simulated directly. The graphite foam heat spreader (PocoFoam®) was bonded directly to the back of the silicon die (Figure 3b) by a technique which utilizes a fluxless solder called S-bond®, i.e. no stackup. This process was performed by the developer of the S-bond technique, Materials Resources International, Inc. (MRi). The silicon die with the foam heat spreader attached was inserted into the PGA package (Figure 3c) and wire bonded with gold bonds at LPS. The wire bonds were protected from vibration by completely encasing the chip cavity (Figure 3e) with an epoxy potting compound (3M DP-270). The PGA was mounted in an aluminum holder with an o-ring groove and attached to the chamber.

The chip assembly (chip, foam, PGA, and PGA holder) was attached to the glass walled chamber flange using #4-40 hex head screws (Figure 3d). An o-ring placed in a groove on the aluminum flange sealed the two components together. At the other end of the fluid chamber, the condenser was mounted and sealed in the same manner. Once the device was assembled, it was mounted in the ZIF socket and locked into place with a lever that allows the socket to firmly grip each pin of the PGA. The fluid chamber has a port with a permanently attached fitting that allows entry of a thermocouple into the chamber and access to the chamber for de-airing. By placing the thermocouple in the vapor space below the condenser, accurate saturation temperatures (T_{sat}) of the fluid can

be obtained.   A valve is also incorporated in this configuration for access for filling, de-airing by boiling, and then sealing for conducting the tests. Figure 3e is a picture of the completed assembly.

The condenser on top of the vapor chamber is an aluminum finned water cooled heat sink. It has fourteen 1/8" x 1" aluminum fins and a water coolant flow of 2 gallons per minutes. Water coolant was held constant at 21C during the tests.
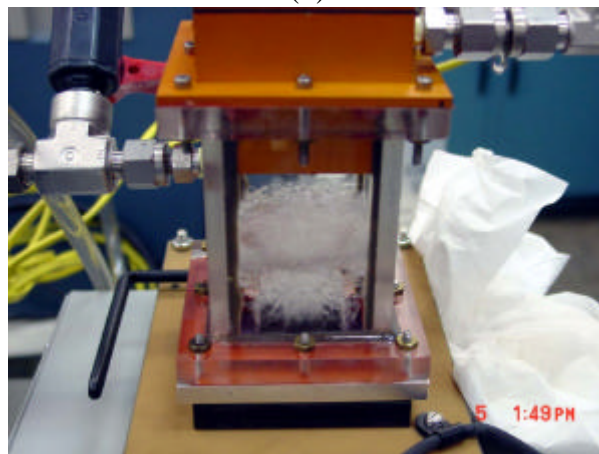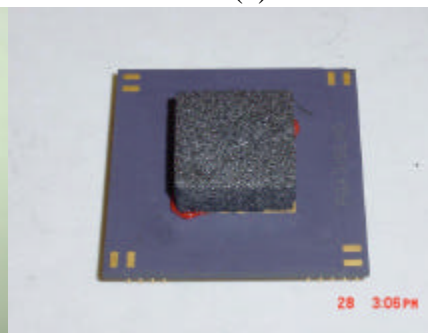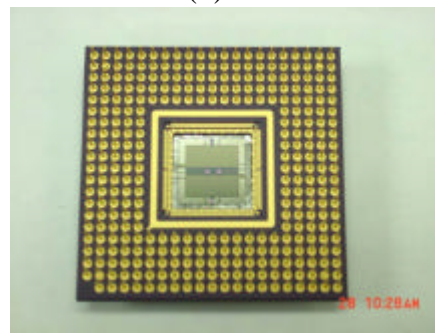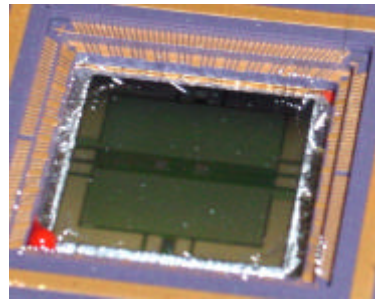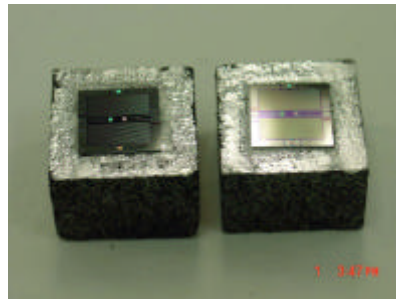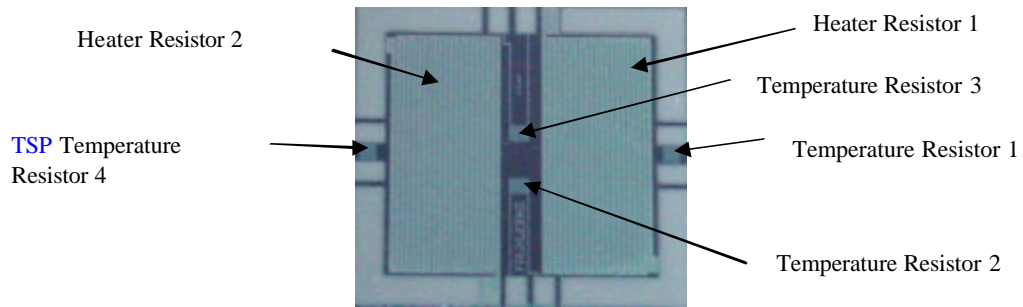
Figure 3. (a) CMOS chip with the resistors for heating and monitoring temperature (b) silicon based CMOS chips bonded to graphite foam blocks, (c) bonded chips inserted into the PGA, (d) wire bonded PGA package (e) evaporative chamber mounted to PGA package.

2.2. Resistor Calibration

The temperature resistors printed on the active layer of the chip are calibrated after assembly of the system. These resistors exhibit a linear correlation between temperature and resistance, thus temperature can be calculated from the resistance measured by a multimeter. First, the system was left at room temperature in a convection oven until the measured resistances came to equilibrium (approximately 15 min). The temperature of the convection oven at the chip was recorded, along with chip resistances. The oven temperature and chip resistances were recorded at thermal equilibrium at several temperatures up to 75°C. This recorded data was used to determine the linear equation of temperature of the active layer (T_{active}) as a function of resistance. This calibration procedure was performed once for each individual chip. Figure 4 shows typical data for a temperature resistor on one chip. The correlation coefficient, R^2, is nearly equal to one, 0.9999, and the resistance is nearly perfectly linear with temperature.
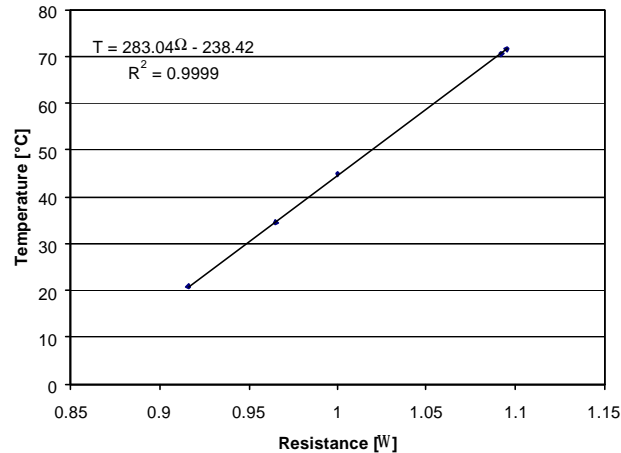

Figure 4.   Plot of temperature of active layer versus resistance of temperature resistor on chip.

2.3 Filling and de-airing the Fluorinert

To fill the system and de-air the Fluorinert, first the inlet and outlet water lines, with inline thermocouples, were attached directly to the condenser using Swagelok fittings. The bubbler, acting as a holding chamber for the Fluorinert, was attached to the fitting on the fluid chamber. Next, the valve was opened causing the fluid level in the chamber to rise to a level equal to the height of the hole.

Fluorinerts are highly oxygenated at atmospheric conditions, and have been used as candidates for artificial blood plasma [18]. A "de-airing" process is necessary to remove the permanent gasses prior to operation. Otherwise, the reduced partial pressure of the Fluorinert will result in higher chip temperatures and superheats. During the de-airing process, heat was added to the chip by simply increasing the current level to the two active resistors in the chip, causing the Fluorinert to boil and release permanent

gasses.   A typical power setting of 20 watts for approximately 30 minutes was used to perform this step.   The permanent gasses were forced through the tube to the collection point. Once the bubbles change shape and form in collection tube and the bubble frequency decreases indicating that the Fluorinert is de-aired, the valve is closed, sealing the system. The level of the fluid in the system can be further adjusted by leaving the valve open to boil away additional fluid.

2.4 Correction for Temperature Rise across Chip

Evaporative cooling systems for cooling chips are typically characterized by plotting the heat flux versus the wall superheat (T_{wall} – T_{sat}) [19].   A heated copper rod is commonly used as a simulant for the actual chip. The interface between the copper rod and the evaporator is used in these cases as the wall temperature (T_{wall}).   A typical stackup, Figure 4, may consist of a silicon chip bonded to a copper-moly shim with epoxy, which in turn was soldered to a copper heat spreader. In this type of stackup, the epoxy layer is the limiting thermal resistance and, hence, this is why manufacturers strive for extremely thin bond lines.   This typical configuration can result in significant temperature rises (T_{active} - T_{wall}) of up to 100°C at the high power densities.   Thus, the temperature of the active layer in a system utilizing these concepts will be extremely high, much above the design limit for reliability of the resistors that the manufacturers specify.
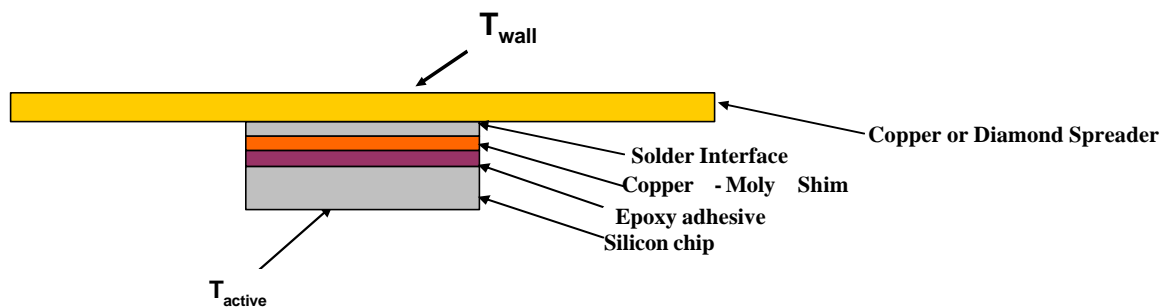

Figure 5.   A typical stack-up of silicon CMOS chips with all of the thermal interfaces identified

In this research, the chip resistor temperatures (T_{active}) are being monitored rather than the back of the foam evaporator (T_{wall}). Even with the graphite foam soldered directly to the silicon die, the temperature rise across the die itself can be significant (Figure 6). A finite element model (Figure 7) was used to model the silicon die, solder interface, and the graphite foam to estimate the temperature gradient through the die. A heat flux, up to 150W/cm^2, was applied to the printed active layer of the silicon die. Figure 8 shows the results at 150 W/cm^2, indicating up to a 30°C temperature rise across the die alone. Figure 9 shows the temperature rise across the die alone versus the power level. To properly compare the results of these tests with previous research, the wall super heat (T_{wall}-T_{sat}) will be calculated based on the temperature at the back side of the evaporator [4-7], not the printed active layer. Therefore, the temperature rise across the

chip ($T_{active} - T_{wall}$) will be subtracted from the measured temperatures (at each heat flux) of the printed active layer to properly reflect a comparable wall temperature.
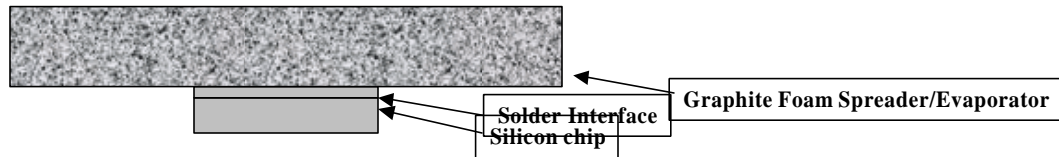

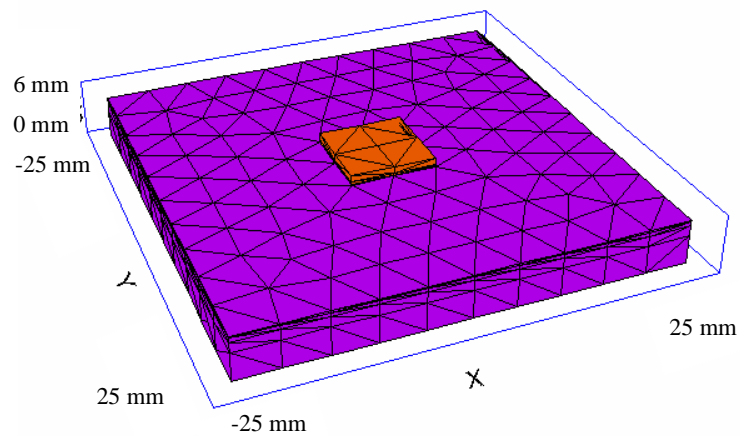Figure 6. The stackup of silicon CMOS chip used in this research

Figure 7.   Finite element mesh for modeling temperature rise across silicon chip during high heat fluxes.
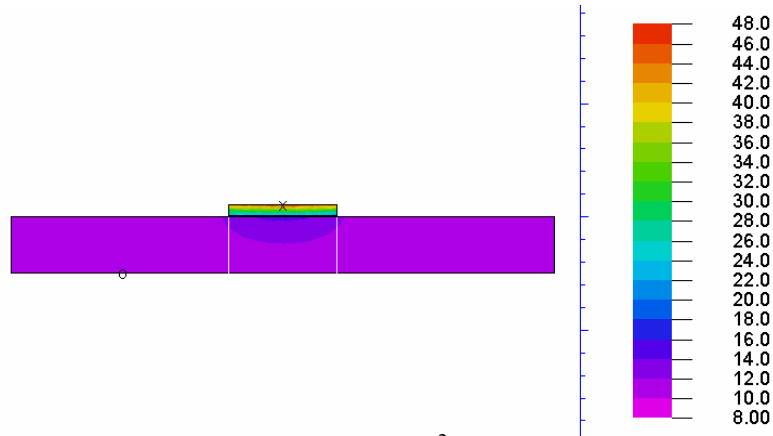
Figure 8. Temperature contours at 150 W/cm^2 across cross-section of system showing up to 30°C temperature rise across silicon die.
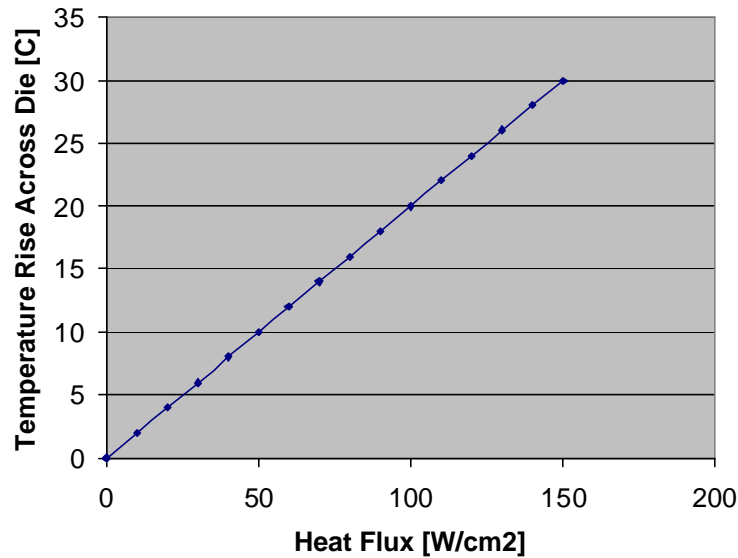

Figure 9. Plot of temperature rise across silicon die for various heat fluxes.

2.5 Experimental procedure

Four chips (1 cm x 1 cm) with different density foams were individually characterized with a baseline run with Fluorinert FC-87 and repeated for validation. Starting at the 20 W power setting, with the valve closed, the cooling water was turned on. Once thermal equilibrium was reached, the power was lowered to 5 W to begin the test. For each power level, the system was allowed to run for 15 minutes to equilibrate and the four resistor levels and T_{sat} were recorded. It is noted that while the cooling fluid temperature was maintained at a constant temperature, the saturation temperature varied with heat flux. The power was increased to 10W, and then in 10W increments until 150 W or chip temperature (active layer) of 90°C was reached.

After the baseline data was obtained, modifications were made to the system including: foam geometry, fluid level, and working fluid type. The results from these changes are described and discussed in the following sections. Table 1 shows the changes made for each chip and Table 2 presents the properties of the foam evaporators and the two fluids evaluated in this study.

Table 1. Variables explored in this paper.

	Foam Density (g/cm³)	Foam Geometry	Boiling Liquid	Fluid Height
Chip 1	ρ = 0.607	Solid	FC-87	3 cm
Chip 2	ρ = 0.602	Solid	FC-87	3 cm
		Solid	FC-72	3 cm
Chip 3	ρ = 0.532	Solid	FC-87	3 cm
		Slotted	FC-87	3 cm
		Thin Layer	FC-87	3 cm
Chip 4	ρ = 0.555	Solid	FC-87	3 cm
		Solid	FC-87	2 cm
		Solid	FC-87	1.2 cm

Table 2a. Fluid Properties [18].

Parameter	symbol	FC-72	FC-87
Molecular Weight [g/mol]	MW	338	288
Melting Point [°C]	MP	-90	-115
Boiling Point [°C]	BP	56	30
Heat of Vaporization [J/kg] (at atmospheric boiling point)	h_{fv}	88000	103000
Liquid Density [kg/m³]	ρ_l	1662	1635
Vapor Density [kg/m³]	ρ_v	13.6	11.6
Kinematic Viscosity [m²/s]	ν	3.61×10^{-7}	2.6×10^{-7}
Surface Tension [N/m]	σ	0.010	0.0089
Liquid Specific Heat [J/(kg·°C)]	C_p	1061	1061
Liquid Thermal Conductivity [W/(m·°C)]	κ	0.057	0.055
Viscosity [kg/m·s]]	μ	0.0006	0.0004
Bond Number	Bo	0.20	0.22

Table 2b. Foam Properties

	Foam 1	Foam 2
Nominal Density	0.60	0.54
Thermal Conductivity	181	~155
Average Cell Size	~300	~350

3. Results and discussion

3.1. *Effect of Evaporator Density.*

The four chips were evaluated to compare the performance of different densities of foam used for the evaporators. As the density of the foam increases, the overall thermal conductivity increases, but the average cell size decreases. As cell size decreases, the ability of the fluid to return to the pores and escape once vaporized will be hindered. When the cells get small enough, capillary action will get stronger and should help the fluid be pulled back into the foam. It was anticipated that there would be a balance between cell size and thermal conductivity to get the most efficient heat transfer. However, the mechanism by which the fluid returns to the pores of the foams after evaporation is unclear. In many microchannel evaporators or even copper wicks for heat pipes, the average cell size is on the order of microns, while the average cell size of the graphite foam is nearly 350 microns. With the much smaller cell size of the other evaporators, the fluid is pulled into the structure with capillary action. The rather large, unique concave cellular structure of the graphite foam may be insufficient to induce capillary action to pull enough fluid into the foam. Instead, the head pressure of the fluid around the foam may simply force fluid into the vacant pores. Perhaps even, the vacuum created as the bubbles escape from the foam pulls fluid back into the foam in other locations (the top or the side), like a pump.

The results of these tests are plotted in Figure 10 and are quite puzzling. As expected, chips 1 and 2, with similar density foams, experienced similar behavior once the superheat reached about 6°C. However, chips 3 and 4, which were made with foams with lower but similar densities, did not behave similarly. Chip 3 displayed higher superheats than chips 1 and 2 at all power densities, while chip 4 displayed lower superheats compared to chips 1 and 2. Possibly, the very nature of the lower density foams is the root cause of the discrepancy in performance between chips 3 and 4. Because the lower density foams exhibit a more open cellular structure, the S-bond may be less consistent compared to the bond for the foams with higher density. The variation in performance may reflect differences in the quality of the bond. Chip 4 seems to have a good thermal interface at the bond while chip 3 may have experienced some failure at the interface during processing

It is unknown why chip 1 and chip 2 diverge in performance at the lower power densities. Notice that chip 4, with the best overall performance, experiences the typical incipience in transfer from convection cooling to pool boiling at about 5 W/cm^2 [6]. It is interesting that the other chips did not display this incipience, yet had poorer performance. Of importance is the comparison of this data to that of a bare silicon die (with no evaporator). The bare silicon die [18] experienced a maximum performance at about 9 W/cm^2 with a superheat of 16 C, compared to chip 4 which displayed a superheat of only 10°C at 100 W/cm^2 (more than an order of magnitude improvement). In addition, compared to Ramaswamy's microchannel evaporator, the graphite foam has a significantly better performance [6].

The typical method of modeling the performance of pool boiling is using an empirical relation with a power law of the following type [19].

$$\frac{q''}{A} = a\left(T_{wall} - T_{sat}\right)^m \qquad\qquad\qquad\qquad \text{(Eq 1)}$$

Typically, the exponent m is in the ballpark of 3-4 [4-6, 18]. However, when fitted to the steady portion of the data in Figure 10 it is found that the exponent m is nearly equal to unity (1.1). This is unexpected because it is generally accepted that the boiling curve for porous evaporators is fairly independent of the evaporator structure.   In traditional microporous metallic evaporators, capillary action is a dominant mechanism controlling wetting, fluid refill, dryout, etc., which all affect boiling performance. Perhaps the unique combination of the high porosity and the extremely high ligament conductivity results in a different mechanism for boiling which is more related to pore structure than capillary action, ultimately allowing higher heat fluxes with a corresponding reduction in slope of the curve.
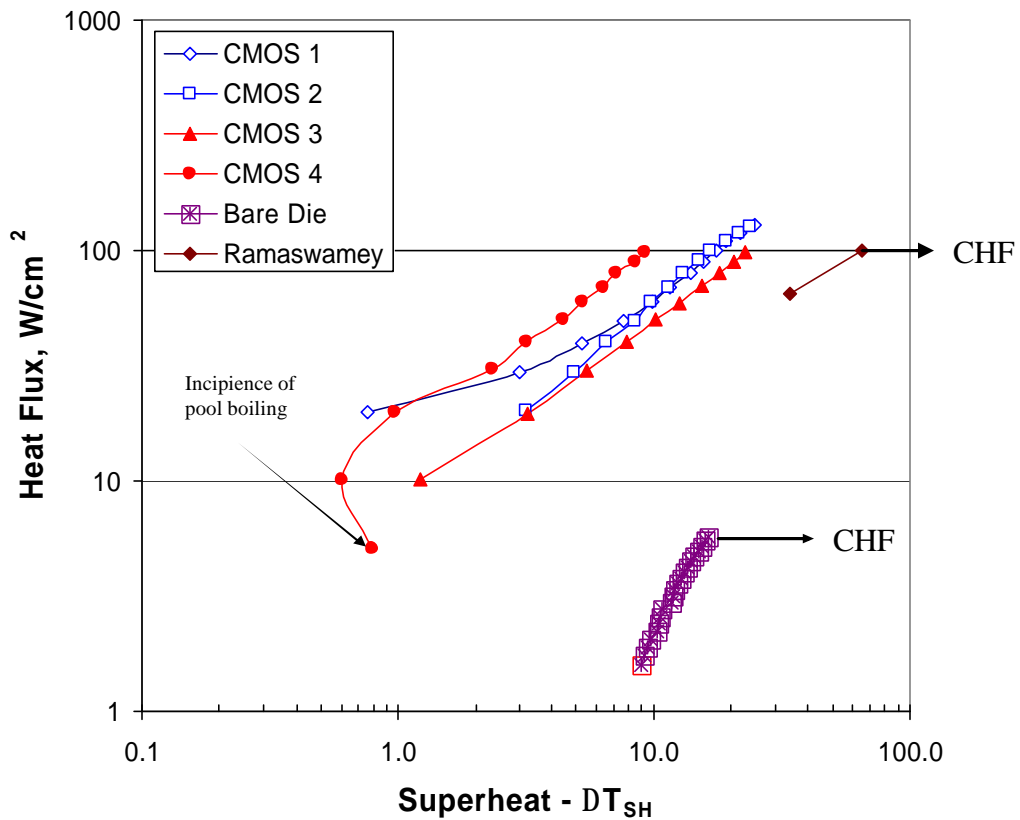

Figure 10.   Plot of heat flux versus degree of superheat for several different graphite foam evaporators compared to a bare silicon die.

Unlike the bare die and Ramaswamey, the graphite foam evaporators do not experience a critical heat flux (CHF) under the conditions tested. The CHF, experienced on the bare die at 16°C, occurs when the rate of vapor generated exceeds that of the fluid

returning to the region of evaporation. When this occurs, the superheat increases very rapidly with a slight increase in heat flux. The lack of CHF for the foam evaporators indicates that a large amount of the surface area within the foam is used for evaporation, lowering the local evaporation rate. Optimization of the foam density and geometry will be critical to maximizing the evaporator performance. It may be possible to reach even higher heat fluxes with the graphite foam and still have very efficient pool boiling.

3.2. Affect of Geometry Modifications

Machining slots into metallic porous evaporators [8] can significantly enhance the performance by up to 3 times. For a solid block of a porous metal, a dry spot can form in the structure just above the die, resulting in no evaporation in this area with only conduction to carry the heat from the die. and an increase in temperature of the die. The slots allow fluid to rush into the center of the foam area, and then wick into the pores of the foam closer to the die, thus reducing temperatures of the die and increasing performance of the system. Therefore, the evaporators for chips 3 and 4 were machined into a slotted pattern (6.25 mm x 6.25 mm) and the performance of the systems were measured. Figure 11 illustrates the machined slotted pattern in Chip 4 (before and after machining).
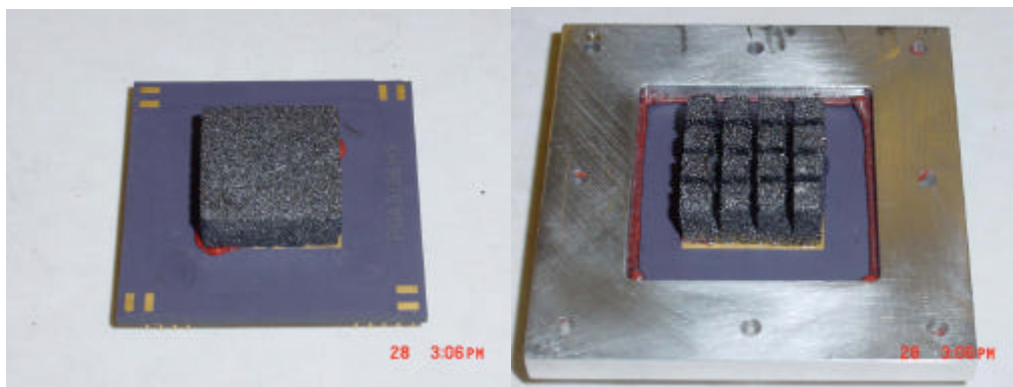

Figure 11.   Images of the graphite foam evaporator bonded to chip 4 with and without machined slots.

Figure 12 shows that for both chips, the slotted geometry pattern produces lower superheats at similar heat fluxes indicating significant performance improvements over the solid evaporator. In fact, chip 4 was able to dissipate 150 W/cm^2 at a modest superheat of only 11°C. Note that the incipience from nucleate boiling to pool boiling in Chip 4 was still around 1-2°C, but the heat flux was increased from about 5 to 40 W/cm^2. The slotted pattern may increase the effectiveness of the convection cooling such that higher heat fluxes can be attained before pool boiling occurs. This improvement is likely

related to the total surface area of the slotted fins. It is also important to note that CHF was not experienced for the slotted foam evaporators.

The most significant result of these tests may be that the actual temperature of the active layer, Figure 13, was less than 71°C for chip 4 and approximately 90°C for chip 3. Therefore this demonstrated that a printed active layer temperature less than the desired 85°C can be attainable at powers as high as 150 W/cm^2 using the graphite foam.
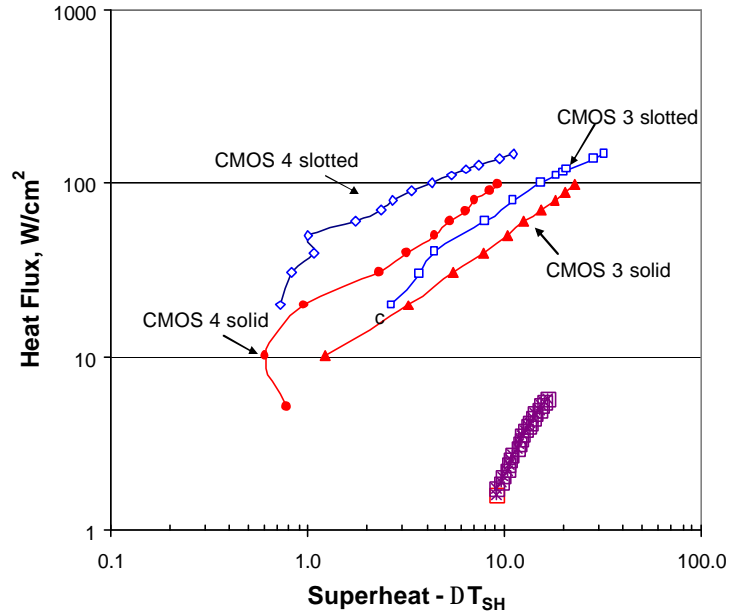

Figure 12.   Plot of heat flux versus superheat for slotted and solid graphite foam evaporators.
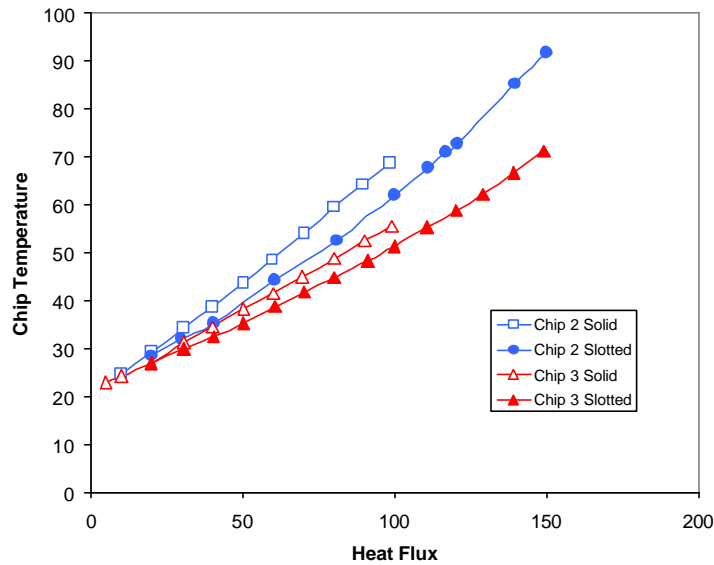

Figure 13.   Plot of temperature of active layer on chip versus heat flux for slotted and solid graphite foam evaporators.

Possibly, the fins are not actually needed and could be removed to yield further improvement, while reducing the overall height of the evaporator. To test this, the slotted section of chip 3 was removed, leaving a thin layer (1 mm) of foam attached to the die. Fig. 14 shows that the thin foam evaporator results in lower performance (but still not CHF) at approximately 100 watts/cm^2 compared to the solid block and slotted foam. The performance of the thin evaporator begins to decrease at between 50 and 60 watts/cm^2 likely due to the significant reduction in surface area, affecting the boiling efficiency. In addition, the reduced height may prevent significant fluid from being sucked into the foam from the sides of the block, resulting in dry out at lower heat fluxes. Also note that the thin layer of foam experienced incipience from nucleate boiling to pool boiling at higher superheats than chip 4. The height to width ratio of the machined slotted fins should be optimized to achieve highest thermal performance of the system.
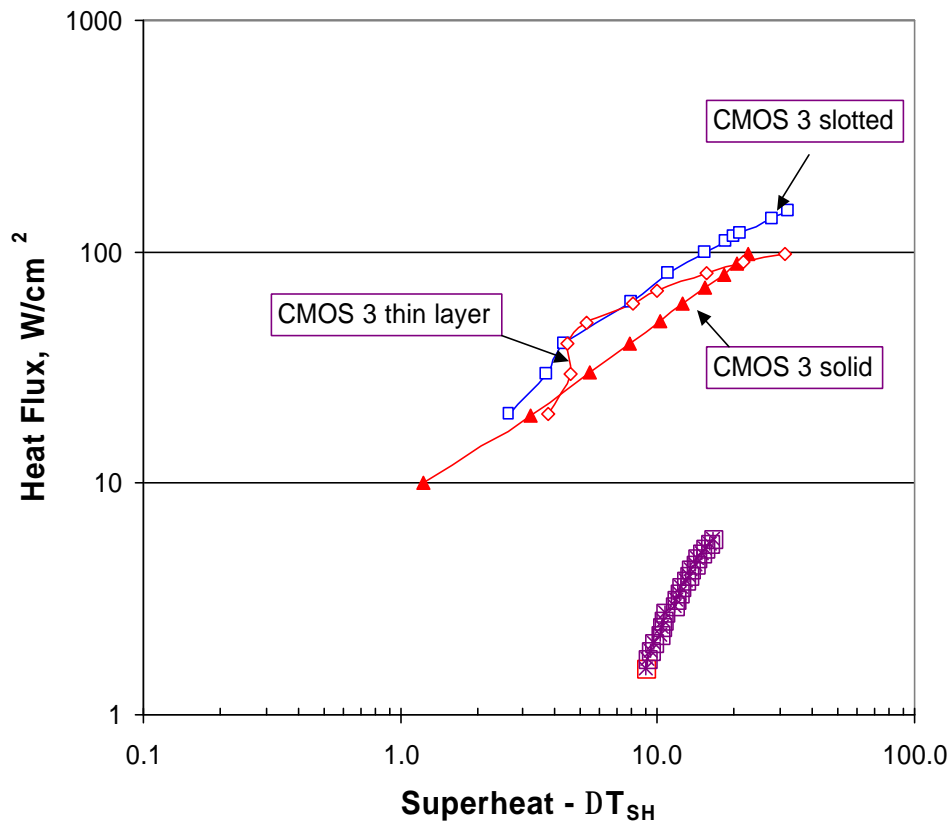

Figure 14.   Plot of heat flux versus superheat for a thin foam evaporator compared with the solid and slotted evaporator for chip 3.

3.3. Fluid Level Analysis

To investigate the effects of fluid head pressure on the system performance, chip 4 was selected for a Fluorinert level experiment. The baseline fluid level was approximately 3 cm (recall that the foam height was 1 cm). After the baseline testing was completed, the chamber was refilled, de-aired and allowed to boil off to a fluid level of 2 cm and finally 1.2 cm (to assure the foam was still completely submerged in fluid at ambient conditions). Fig. 15 shows that the thermal performance for the three fluid levels were nearly identical indicating that fluid level does not significantly affect the performance of saturation pool boiling.
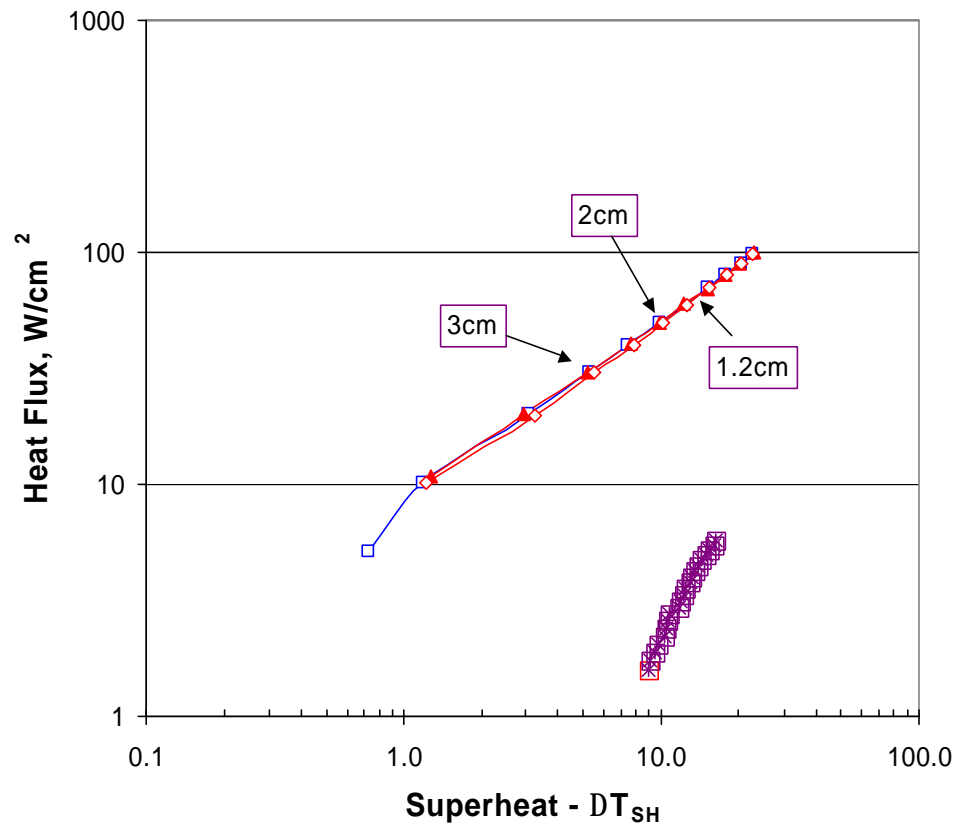

Figure 15. Plot of heat flux versus superheat for three different levels of Fluorinert.

3.4. Working Fluid Analysis

Chip 2 was tested using Fluorinert FC-72, in addition to the baseline FC-87, to characterize the effects of the boiling temperature of the working fluid on the system performance. The results in Fig. 16 show that using FC-72 produces very similar superheats as the FC-87 at power settings less than 60 watts. However, at 60 watts the FC-72 starts yielding indicating initial signs of a critical heat flux, which is anticipated [4-8]. It is important that traditional models of pool boiling do not take into account the fluid in the equation, with the exception of the calculated coefficients. It was observed here that the fluid has a slight effect, albeit not statistically significant (further research

will be required to verify this). This indicates that the traditional models are appropriate as the small changes due to the fluid will be incorporated into the equation during the fitting of the exponents and coefficients.
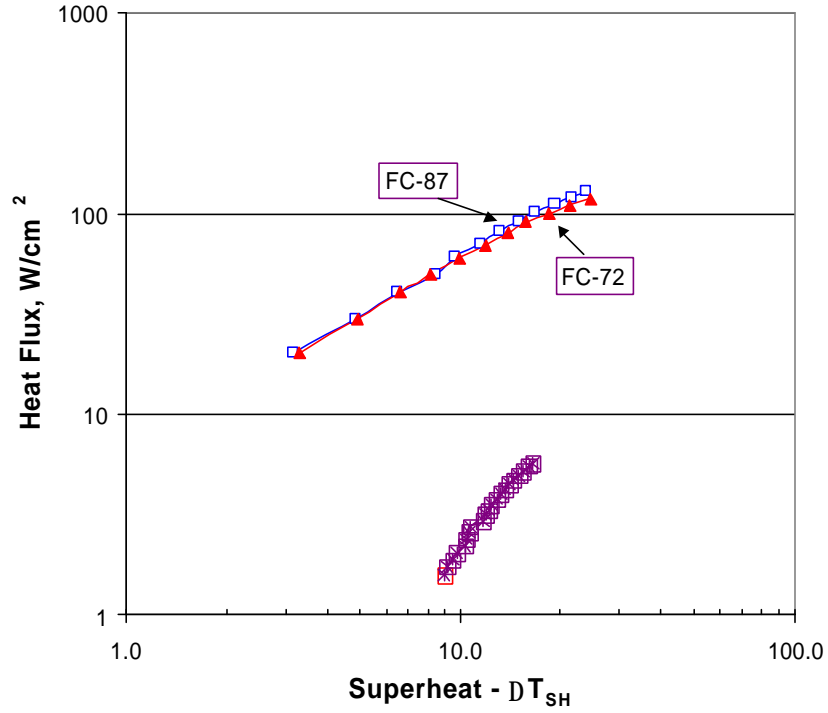

Figure 16.   Plot of heat flux versus superheat for two types of Fluorinert.

The reduction in performance of FC-72 can be explained by looking at the differences in properties of FC-87 and FC-72 including heat of vaporization, liquid and vapor densities, and viscosity. The following equations can be used to investigate the effect of these differences.

$$Bo = \frac{\boldsymbol{b}(\boldsymbol{r}_v - \boldsymbol{r}_l)d^2{}_{pore}}{\boldsymbol{s}} \qquad \text{(Eq 2)}$$

$$Gr = \frac{g\boldsymbol{b}(T_{wall} - T_{sat})d^3{}_{pore}}{v^2} \qquad \text{(Eq 3)}$$

$$C_a = \frac{\boldsymbol{mu}}{\boldsymbol{s}} \qquad \text{(Eq 4)}$$

The bond number (*Bo*) indicates the ratio of buoyancy to surface tension forces during pool boiling. Using the properties listed in Table 2 and a typical pore diameter of 350 µm, the bond numbers for FC-87 and FC-72 are 0.22 and 0.20 respectively. A lower bond number in the FC-72 indicates that bubbles have to overcome a larger surface tension force before departure.

Since the Grashof number and the capillary number are dependent on superheat temperatures and velocity, respectively, data from boiling FC-87 is used in the following calculations. For a heat flux of 149 W, a cross sectional area of the foam of 2.5 by 2.5 cm, and a superheat of 11C, the Grashof number (*Gr*), ratio of buoyancy to viscous forces, was calculated to be 102.

In order to use the capillary number (*Ca*), ratio of viscosity to surface tension forces, for further investigation, the liquid and vapor velocities must be calculated. Using the equation below, the liquid and vapor velocities for FC-87 are calculated to be 0.14 cm/s and 19.46 cm/s respectively.

$$u_{v,l} = \frac{q''}{\rho_{v,l} A_c h_{fg}},$$ (Eq 5)

where q is the total heat flux. Then, using the liquid velocity, the capillary number for FC-87 is calculated to be 6.2 x 10^{-5}.

These non-dimensional numbers indicate that viscosity forces (Ca) compared to surface tension (Gr) and buoyancy forces (Bo) are of little significance, and FC-87 with more a favorable (lower) surface tension should experience higher CHF's. Hence, for high power systems, FC-87 would be the fluid of choice if the cooling temperature is less than the boiling temperature of 30°C. However, if the ambient cooling temperature is higher than 30°C, then FC-72 would be preferred.

3.5. Overall Thermal Resistance and Heat Transfer Coefficient

One method to evaluate different cooling techniques is to compare the boiling thermal resistances, defined as the ratio of superheat ($T_{wall} - T_{sat}$) to the total heat duty, q''.

$$R_{boil} = \frac{(T_{wall} - T_{sat})}{q''},$$ (Eq 6)

The resistances to boiling for the graphite foam thermosyphons are significantly better than for other pool boiling techniques (Table 3). Ideally, by optimizing both the evaporator and condenser designs, the thermal resistance of the foam based systems should improve. For example, incorporation of graphite foam on the condenser side may provide improvements to the overall thermal resistance.

Table 3 also shows the effective boiling heat transfer coefficient ($h_{eff,boil}$) with various porous evaporators compared to the graphite foam thermosyphons. The graphite foam exhibits effective heat transfer coefficients significantly greater than that of other porous evaporators, once again indicating the effectiveness of the high thermal conductivity combined with the high surface area to increase the evaporation rate. In fact, the graphite foam thermosyphons performed significantly better than spray cooling with FC-72. Only when water was utilized as the fluid, did spray cooling dissipate more heat than the graphite foams. However, the graphite foams still yields a boiling thermal resistance better than that of spray cooling, regardless of the fluid. This is significant as the graphite foam thermosyphons have no moving parts, no spray nozzles that can be clogged, no pumps, etc. that can reduce reliability and increase costs. The heat transfer coefficient is defined as:

$$h_{eff} = \frac{q''/A}{\Delta T_{SH}},$$
(Eq 7).

Table 3. Heat transfer performance of state-of-the-art thermosyphons and spray cooling techniques found in literature compared to that of the graphite foam thermosyphons.

Reference	Evaporator	Fluid	Heat Flux, q''	ΔT_{SH}	R_{boil} ($\Delta T/q''$)	$h_{eff,boil}$
3M [18]	None	FC-87	5.7[†]	16.4	2.88	3476
El-Genk [9]	Copper Surface	HFE-7100	22[†]	28	1.27	7857
Wei et al.[8]	Sintered Bronze Powder	R11	40[†]	40	1.00	10000
Ramaswamy [6]	Microchannel copper	FC-72	100[†]	65	0.65	15384
Rainey & You [4]	Microporous Diamond (DOM)	FC-72	27[†]	13	0.48	20769
Lin and Ponnappan [2]	**SPRAY COOLING**	FC-72	78[†]	38	0.48	20526
Nakayama [10]	Microchannel copper	FC-72	159[†]	65	0.41	24461
Coursey [7]	Poco HTC High Density Foam	FC-87	142.6[‡]	51.2	0.36	27581
Rainey and Lee [5]	Pin Finned Copper Block w/ Microporous Aluminum Coating	FC-72	140[†]	38	0.27	36842
This research	PocoFoam®	FC-72	118[‡]	24	0.20	49167
Lin and Ponnappan [2]	**SPRAY COOLING**	Water	480[†]	48	0.1	100000
This research	Slotted PocoFoam®	FC-87	149[‡]	11	0.07	135455

[†] CHF reached

[‡] CHF not reached

Figure 17 is a plot of the boiling thermal resistance for various microporous evaporators versus heat flux. One interesting aspect of the plot is that each of the designs (including no evaporator), except the graphite foam based evaporators, follow an asymptotic relationship and seem to be independent of fluid and the mircoporous evaporator itself. This trend is expected because the models for boiling do not include the fluid parameters or the porosity of the evaporators, only superheat and heat flux. This reinforces the idea

that the graphite foams allow a different mechanism to govern boiling. Perhaps due to the high surface area and ligament conductivities, the performance of the graphite foam evaporators is limited by a mechanism other than the boiling characteristics of the fluid In any event, the graphite foam is a departure from typical materials used as evaporators and represents a unique opportunity to improve heat transfer.
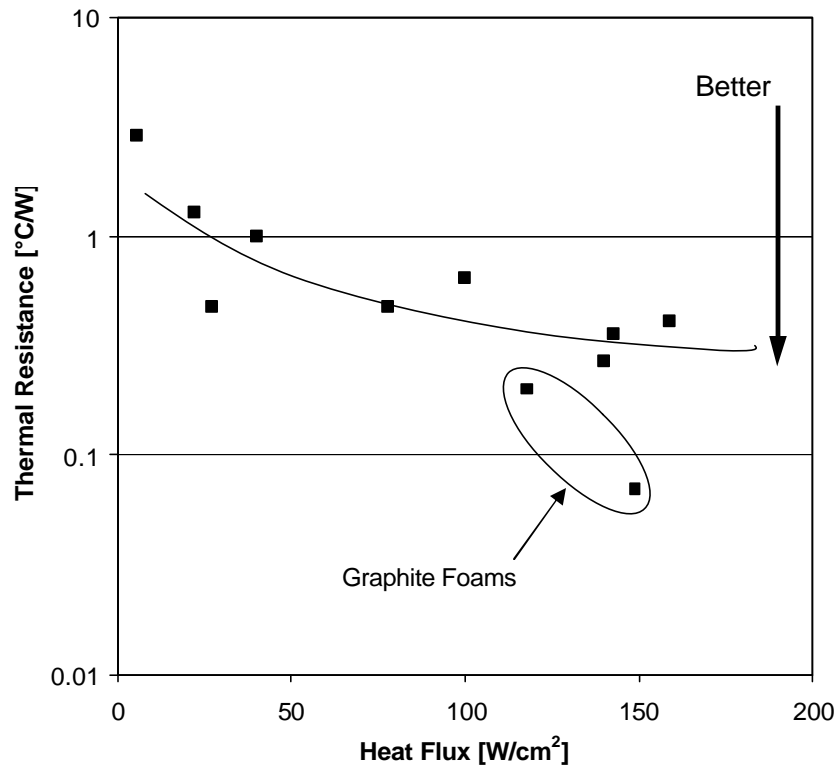

Figure 17.   Plot of thermal resistance versus degree of superheat for various microporous evaporators and fluids used in thermosyphons.

4. Conclusions

It is clear that the density of the foam evaporators affect the thermal performance of the system. In one case, foam with a lower density performed significantly better than a higher density foam. However, the mechanism for the improvement is not fully understood. Perhaps a more open structure allows more fluid to return faster to the pores of the foam for evaporation, thus enhancing performance. However, at some minimum density, the decrease in thermal conductivity will probably become the dominant mechanism and a decrease in performance will occur.

In addition, the fluid level and fluid type had very little effect on the overall performance in the system, which makes fabrication of a commercial device less challenging. Fortunately, a wide variety of fluids exist with different boiling points which permits tailoring of a system for different power requirements.

Modifying the foam structure to enhance the rate of return of fluid to the foam closest to the die can significantly improve the performance. With a slotted foam evaporator, a heat flux of 150W/cm^2 resulted in wall superheats of only 11°C. Many other geometries, such as the introduction of large channels (drilled holes, both horizontal and vertical) may be suitable and could even enhance performance.

The experimental setup used in this research gives accurate measurements of the actual active layer in the chip. Active layer temperatures less than 71°C have been achieved at heat fluxes of 150 W/cm^2. This performance is significantly better than any prior literature data. In fact, the graphite foam thermosyphons resulted in a better boiling thermal resistance (and heat transfer coefficient) than spray cooling. It is very important to note that as the temperature of the chips rise by 10C, the life is reduced roughly in half [BSL]. The Arrhenius equation predicts that the rate of reaction (i.e. component breakdown) doubles with each 10C increase in temperature. Thus, the graphite foam thermosyphons have the ability to increase life and reliability of microprocessor while increasing power levels of the chips.

Since, water has been shown to perform significantly better than fluorocarbons [2], perhaps, if the foams could be treated properly such that they wet readily with water, then the graphite foam thermosyphons can be utilized for extremely high power densities, at a much lower cost to spray cooling.

One very important note is that critical heat flux was not reached in these experiments with graphite foam evaporators. In all literature surveyed, CHF was reached, thus giving the limiting conditions for operation. It is anticipated that this ability to extend the critical heat flux will lead to further increases in performance of these systems.

Finally, use of the foam in the condenser area of the system offers the possibility of gaining similar improvements to the performance of these evaporative cooling devices. Condenser modifications will be the focus of further research.

5. Acknowledgements

6. Nomenclature

T_{wall} = temperature of the interface between the evaporator and silicon chip [°C]

T_{active} = temperature of the active layer on silicon chip [°C]

T_{sat} = temperature of the fluid in the system [°C]

R_{boil} = boiling thermal resistance [°C/W]

$h_{eff,boil}$ = effective boiling heat transfer coefficient [W/m²K]

Gr = Grashof Number, (ratio of buoyancy to viscous forces)

Bo = Bond Number, (ratio of buoyancy to surface tension forces)

Ca = Capillary Number, (ratio of viscous to surface tension forces)

C_p = specific heat of fluid [J/kg]

ν = kinematic viscosity of fluid [m²/s]

q'' = heat load on chip [W]

μ = viscosity of fluid [m/s]

σ = surface tension of fluid [N/m]

ρ = density of fluid [g/cm³]

β = Thermal expansion coefficient [1/°C]

g = acceleration due to gravity [m/s²]

d_{pore} = average diameter of cells in foams [m]

A = cross sectional area of vapor chamber [m²]

h_{fg} = latent heat of vaporization of fluid [J/kg]

ΔT_{SH} = degree of wall superheat [°C], (T_{wall}-T_{sat})

$u_{v,l}$ = velocity of coolant vapor or coolant liquid within evaporator[m/s]

7. References

[1] ISR, "www.spraycool.com," Isothermal Systems Research, 2003.

[2] L. Lin and R. Ponnappan, "Heat Transfer Characteristics of Spray Cooling in a Closed Loop," *Int. J. Heat Mass Transfer*, vol. 46, pp. 3737-3746, 2003.

[3] S. B. Memory, D. C. Sugiyama, and P. J. Marto, "Nucleate Pool Boiling of R-114 and R114-oil Mixtures from Smooth and Enhanced Surfaces - 1. Single Tubes.," *Int. J. Heat Mass Transfer*, vol. 38, pp. 1347-1361, 1995.

[4] K. N. Rainey and S. M. You, "Effects of heater size and orientation on pool boiling heat transfer from microporous coated surfaces," *International Journal of Heat and Mass Transfer*, vol. 44, pp. 2589-2599, 2001.

[5] K. N. Rainey, S. M. You, and S. Lee, "Effect of pressure, subcooling, and dissolved gas on pool boiling heat transfer from microporous, square pin-finned surfaces in FC-72," *International Journal of Heat and Mass Transfer*, vol. 46, pp. 23-35, 2003.

[6] C. Ramaswamy, Y. Joshi, and W. Nakayama, "Combined Effects of Sub-Cooling and Operating Pressure on the Performance of a Two-Chamber Thermosyphon," *IEEE Transactions on Components, Packaging, and Manufacturing Technology-Part A*, pp. 61-69, 2000.

[7] J. Coursey, "Performance and Parametric Investigation of a Graphite Foam Thermosyphon Evaporator," in *Mechanical Engineering*. College Park: University of Maryland, 2003, pp. 93.

[8] W. Wu, J.-H. Du, X.-J. Hu, and B.-X. Wang, "Pool boiling heat transfer and simplified one-dimensional model for prediction on coated porous surfaces with vapor channels," *International Journal of Heat and Mass Transfer*, vol. 45, pp. 1117-1125, 2002.

[9] M. S. EL-Genk and H. Bostanci, "Saturation boiling of HFE-7100 from a copper surface, simulating a microelectronic chip," *International Journal of Heat and Mass Transfer*, vol. 46, pp. 1841-1854, 2003.

[10] W. Nakayama, T. Nakajima, and S. Hirasawa, "Heat Sink Studs Having Enhanced Boiling Surfaces for Cooling Microelectronic Components," *ASME Paper*, 1984.

[11] P. Boudreaux and J. Latondre, "Laboratory for Physical Sciences," 2000.

[12] J. Klett, "High Thermal Conductivity, Mesophase Pitch-Derived Carbon Foam," presented at Proceedings of the 1998 43rd International SAMPE Symposium and Exhibition, Part 1 (of 2), Anaheim, California, U.S.A., 1998.

[13] J. Klett, "High Thermal Conductivity, Mesophase Pitch-Derived Graphitic Foams," *Journal of Composites in Manufacturing*, vol. 15, pp. 1-7, 1999.

[14] J. Klett, "Pitch Based Carbon Foam and Composites." USA: UT-Battelle, LLC, 2002.

[15] J. Klett, "Process for Making Carbon Foam." U.S.: Lockheed Martin Energy Research Corporation, Oak Ridge, Tennessee, 2000.

[16] J. Klett, R. Hardy, E. Romine, C. Walls, and T. Burchell, "High-Thermal-Conductivity, Mesophase-Pitch-Derived Carbon Foams: Effect of Precursor on Structure and Properties," *Carbon*, vol. 38, pp. 953-973, 2000.

[17]   J. Klett, A. D. McMillan, N. C. Gallego, and C. A. Walls, "The Role of Structure on the Thermal Properties of Graphitic Foams," *Journal of Material Science*, vol. In Press., 2004.

[18]   L. Tousignant, "3M Database," 2004.

[19]   W. L. McCabe, J. C. Smith, and P. Harriott, *Unit Operations of Chemical Engineering*. New York: McGraw-Hill, 1985.